Transition densities and form factors in the triangular α-cluster model of ^{12}C with application to $^{12}\mathrm{C}+\alpha$ scattering

A. Vitturi,[1,2] J. Casal,[1,2] L. Fortunato,[1,2] and E. G. Lanza[3,4]
[1]*Dipartimento di Fisica e Astronomia "G. Galilei", Università di Padova*
[2]*I.N.F.N., Sez. di Padova, I-35131 Padova, Italy*
[3]*I.N.F.N., Sez. di Catania, I-95123 Catania, Italy*
[4]*Dipartimento di Fisica e di Astronomia "Ettore Majorana", Università Catania, Italy*

(Received 1 October 2019; published 21 January 2020)

Densities and transition densities are computed in an equilateral triangular α-cluster model for ^{12}C, in which each α particle is taken as a Gaussian density distribution. The ground state, the symmetric vibration (Hoyle state), and the asymmetric bend vibration are analyzed in a molecular approach and dissected into their components in a series of harmonic functions, revealing their intrinsic structures. The transition densities in the laboratory frame are then used to construct form factors and to compute distorted-wave Born approximation inelastic cross sections for the $^{12}\mathrm{C}(\alpha,\alpha')$ reaction. The comparison with experimental data indicates that the simple geometrical model with rotations and vibrations gives a reliable description of reactions where α-cluster degrees of freedom are involved.

DOI: 10.1103/PhysRevC.101.014315

I. INTRODUCTION

Few nuclear systems have attracted the interest of the scientific community as the ^{12}C nucleus, which is remarkable in many respects: It is the nucleus at the center of the atom mostly associated with life on earth and yet it is produced in the billion-kelvins hot plasma of stars. It is a crucial $N=Z$ even-even system that shows an unusual energy spectrum and rotational bands and despite the large number of experiments, various theoretical interpretations of data, and a handful of models of its nuclear structure, it escapes conventional descriptions such as the single-particle shell model or the collective model. In particular, it still largely baffles the efforts of pinning its structure down with *ab initio* nuclear shell model based on realistic interactions, due to the strong tendency of nucleons to form clusters of α particles. This is a signal that even the most up-to-date nucleon-nucleon (NN) interactions still miss some important ingredient that could explain clusterization in light nuclei. Reactions involving ^{12}C as a target or as a projectile have been performed extensively because it is easy to chemically or physically deal with this abundant isotope in order to produce targets or to build ion sources that can deliver intense ion beams. The acceleration of these ions to various energies allows the analysis of several types of reactions that highlight different aspects worthy of interest, like cluster transfer reactions, nuclear rainbow, and a number of studies aimed at measuring the nuclear S factor that is relevant for astrophysics.

A large number of models have been constructed over the years with several degrees of success that cover various aspects of its complex phenomenology, but a final word has not yet been written [1–3]. Very interestingly, instead of going into the direction of treating the system of $A=12$ particles with individual degrees of freedom, another line of investigation has been recently pursued, the Algebraic Cluster Model [4–12], in which a simplification in terms of rotational and vibrational excitations of an equilateral triangular configuration of three α particles seems to offer a valid explanation of most of the low-energy spectral features of ^{12}C. These kinds of molecular models have a long history, starting with Wheeler in 1937 [13–16] and have been forgotten or misunderstood in the past and left behind in favor of fully microscopic approaches. Notably, the criticisms contained in the book by Blatt and Weisskopf [17], which were certainly well-grounded but have been surpassed by new accumulated knowledge, have contributed to belittle this approach. On the other hand, it is true, that light nuclei, those that bridge the gap from deuterium to the mass region where the single-particle shell model starts to work beyond any doubt, have been subject to profound investigations both from the theoretical and experimental sides that support a molecular-like interpretation. A very important experimental work with a strong theoretical foundation was done by W. von Oertzen and coworkers which identified several molecular structures and rotational bands with certainty [18–21] and they formulated a molecular orbital theory, inspired by quantum chemical models, for the bonds of additional neutrons that move in the force fields of α-cluster structures. These structures, quite similarly to what happens in molecules, can vibrate and rotate around fixed positions, but, quite differently to what happens in molecules, are not rigid at all. They rather are soft dynamical nuclear systems, whose zero point motion has the same size of the nucleus itself, and therefore the underlying geometric configurations should be attributed to equilibrium points around which large fluctuations occur (in other words, the Born-Oppenheimer approximation does not work here). Rotations and vibrations

have approximately the same energy scales and they are intertwined with stronger ties.

Linear chains of α particles [22] as well as Bose-Einstein condensate (BEC) gas of α bosons [23] have been proposed as possible explanations of certain states or parts of the energy spectrum. The literature is rich with theoretical interpretation: cluster models (e.g., Ref. [24]), No-Core Shell Model (e.g., Refs. [25,26]), as well as Antisymmetrized Molecular Dynamics (e.g., Ref. [27]), Fermion Molecular Dynamics [28,29], Effective Field Theory [30] and lattice calculations (e.g., Ref. [31]), and Nonlocalized Clustering [32], each with its own merits. A lucid analysis of all these models [1] reveals, however, that no final agreement can be reached for the underlying geometric structure. Recently, one of us [33] proposed a theoretical scheme based on discrete point-group symmetries, by which a Raman fluorescence experiment in which the depolarization ratio is measured for the excited states might discriminate among all possible types of geometric configurations with certainty, thus offering a solution to this conundrum.

We have dealt with nuclear structure until now, but reactions of ^{12}C are of paramount importance, because, leaving aside the interest in understanding and modeling the reaction mechanisms themselves, it is through dynamical processes like collisions and absorption or emission of electromagnetic waves that we have a handle on the structural features, from which one could ultimately derive fundamental information on the nuclear interactions. Thus, it appears to us that some blending of these two wide chapters of physics has to be done and our chosen method will be that of transition densities. One of the earliest works in this respect, and very similar in spirit to ours, though based on a resonating group method calculation, was that of Kamimura [34]. A folding-model analysis of the inelastic $^{12}\mathrm{C}+\alpha$ scattering has been performed in Ref. [35] using Antisymmetrized Molecular Dynamics to calculate wave functions and transition densities and using either the distorted-wave Born approximation (DWBA) or coupled channels to compute the differential cross sections. More recently, Ito [36] linked the coupled-channels fit of inelastic scattering data to the extended nature of the 2_2^+ state in the Hoyle band. Even more recently, Kanada-En'yo and Ogata came up with a reanalysis of the α-scattering cross sections in a coupled-channels formalism [37]. In this reference the monopole and dipole excitations and several other observables are discussed and in the conclusions it is stated that further calculations are required to reduce the ambiguities of several parameters entering the structure calculations.

We have given a preliminary account of some of the features of our approach in Ref. [38]. Therefore in the present paper we will proceed to investigate various aspects of structure and reactions in connection with the occurrence of α clusters in the ^{12}C nucleus. We will begin by studying the equilateral triangle model and its density and transition densities not only for the ground-state band but also for excited vibrational bands. Then we will use it to calculate form factors between these states and these, in turn, will be used to compute inelastic scattering cross sections in DWBA. Our main aim is to show that a simple description in terms of rotations and vibrations of triangular configurations is sufficient to yield all the relevant features of the inelastic process. While complicated models including *NN* interactions are certainly more advanced, they are not necessary to describe the most salient features of this process. A simple model based on symmetry accounts for practically all of the relevant facts.

II. DENSITIES AND TRANSITION DENSITIES

The density of the α particle is taken as a Gaussian function:

$$\rho_\alpha(\vec{r}) = \left(\frac{\alpha}{\pi}\right)^{3/2} e^{-\alpha r^2}, \tag{1}$$

with $\alpha = 0.56(2)$ fm^{-2} as in Refs. [4,5]. The three-dimensional spherical integral of this function is normalized to 1; therefore one should always multiply by 2 (the charge of an α particle) when dealing with charge-related quantities and multiply by 4 (the mass of an α), when dealing with mass-related properties. Now, with the aim of constructing the density of ^{12}C as a sum of three α particles placed at the vertices of a triangle, each particle should be displaced of the proper amount, β, and therefore we have

$$\rho_{\mathrm{gs}}(\vec{r}, \{\vec{r}_k\}) = \sum_{k=1}^{3} \rho_\alpha(\vec{r} - \vec{r}_k), \tag{2}$$

with $\vec{r}_1 = (\beta, \pi/2, 0)$, $\vec{r}_2 = (\beta, \pi/2, 2\pi/3)$, and $\vec{r}_3 = (\beta, \pi/2, 4\pi/3)$ in spherical polar coordinates (r, θ, ϕ), where the colatitude is always $\pi/2$ because we have chosen a triangle lying in the $\{xy\}$ plane with the particle labeled as 1 on the positive x axis. Once the angular position of the α particles has been decided, the dependence on the nine variables contained in the three vectos $\{\vec{r}_k\}$ is reduced to the single radial variable that we have called β. With the proviso made above, the integral of this density is normalized to 3, and therefore, once again, one should properly multiply by 2 or 4 depending on the aim of the calculations. The shape of this "static" ground-state density, labeled gs, is associated with the fully symmetric representation, A, of D_{3h} with 0 quanta of excitation [11,12]. In the following, β will be set to a constant value; therefore the explicit dependence on it can be dropped. Thus the density can be expanded in spherical harmonics as

$$\rho_{\mathrm{gs}}(\vec{r}) = \sum_{\lambda\mu} \rho_{\mathrm{gs}}^{\lambda,\mu}(r) Y_{\lambda,\mu}(\theta, \varphi), \tag{3}$$

where $\rho_{\mathrm{gs}}^{\lambda,\mu}$ are the intrinsic radial transition densities that depend on λ, μ. Our choice of coordinates is such that only those multipoles that are allowed by the D_{3h} symmetry appear in the sum. This is different from Ref. [4] where the z axis was instead chosen to pass through particle 1 and the center of the triangle. In setting up this model and Eqs. (1)–(3), we did not worry about the effect of the Pauli exclusion principle, which is expected to generate some repulsion between the α's at short distances, because of the phenomenological nature of our approach. This repulsion can be simulated with a change in the effective densities for overlapping particles, which should not appreciably affect the profile of densities and transition densities on the tails, where they are important

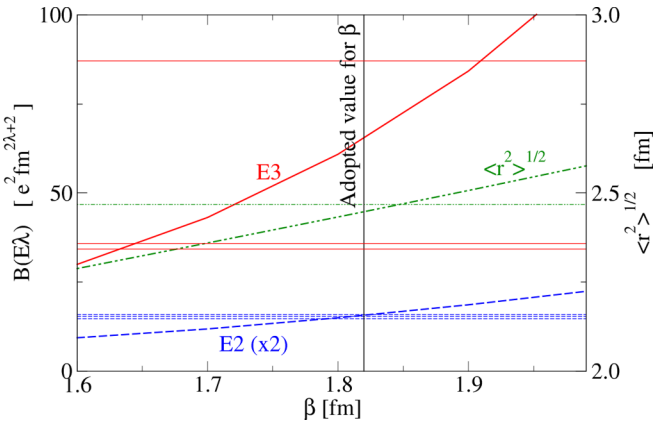

FIG. 1. Calculated values of $B(E2;2_1^+ \to 0_1^+)$ (dashed) and $B(E3;3_1^+ \to 0_1^+)$ (solid) are shown as blue and red thick lines, while experimental values (without error bands) are shown as light horizontal lines of the same color and type. Units are on the left vertical axis; notice that the $E2$ has been multiplied by two. We plot in green dot-dashed lines the rms radius and only one experimental value for reference (units on the right vertical axis). The black vertical line at $\beta = 1.82$ marks the value adopted in this paper.

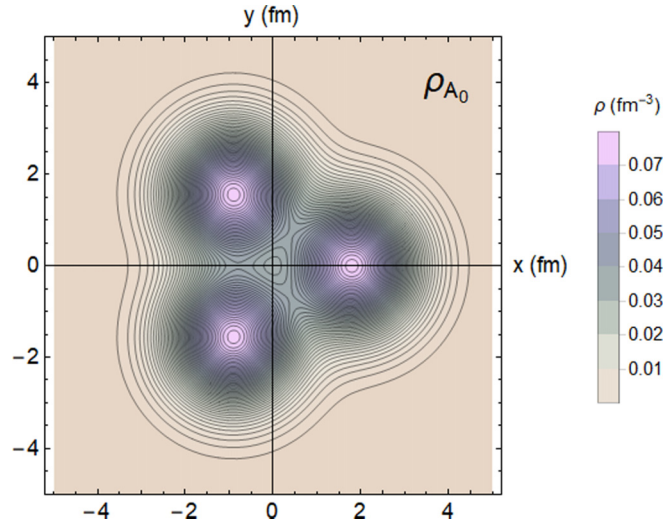

FIG. 2. Contour plot of density in fm^{-3} (cut on the $z = 0$ plane), $\rho_{\rm gs}$ in Eq. (2), of the ground-state static triangular configuration (with A symmetry).

for reaction calculations. Once the densities are known in the intrinsic frame, they should be transformed into the laboratory frame, where the dependence on μ is lost. Details on how to accomplish this are given in the Appendix. The laboratory-frame radial transition densities allow the calculation of several intraband observables, such as the reduced electromagnetic transitions $B(E\lambda)$ in terms of the corresponding matrix elements $M(E\lambda)$ defined as:

$$M(E2;2_1^+ \to 0_1^+) = Z \int \rho_{\rm gs}^{\lambda=2}(r) r^4 dr, \tag{4}$$

where $Z = 2$ is the charge of a single α particle and more generally,

$$M(E\lambda;\lambda \to 0_1^+) = Z \int \rho_{\rm gs}^{\lambda}(r) r^{(\lambda+2)} dr, \tag{5}$$

$$B(E\lambda;\lambda \to 0_1^+) = \frac{1}{2\lambda+1} \mid M(E\lambda;\lambda \to 0_1^+) \mid^2, \tag{6}$$

and the diagonal matrix elements and root-mean-square radius defined as:

$$M(E0) = \sqrt{4\pi} Z \int \rho_{\rm gs}^{0}(r) r^4 dr, \tag{7}$$

$$\langle r^2 \rangle_{0_1^+}^{1/2} = \left[\sqrt{4\pi} \int \rho_{\rm gs}^{0}(r) r^4 dr / \mathcal{N} \right]^{1/2}, \tag{8}$$

where $\mathcal{N} = \sqrt{4\pi} \int \rho_{\rm gs}^{0}(r) r^2 dr = 3$ is a normalization integral that just counts the number of α particles.

Now one might take the radial parameter for distance as $\beta = 1.74(4)$ fm for $k = 3$ clusters as in Ref. [4,5], but we prefer to choose $\beta = 1.82$ fm because this allows us to fix both the ground-state radius and the $B(E2)$ to the first excited 2^+ state. The change of calculated values with β is compared with available experimental data in Fig. 1. Horizontal colored lines are measurements, while the vertical black line is the adopted value, i.e., a compromise between $B(E2)$ and the root-mean-square radius. Experimental values for $B(E3)$ are either too small or too large and in any case they do not agree with each other, but our adopted value falls in the middle.

Returning now to the density defined above, Fig. 2 shows a contour plot of the static triangular configuration associated with the ground-state band, while Fig. 3 shows the three lowest-order radial functions of the expansion in spherical harmonics for $\{\lambda\mu\} = \{00, 20, 33\}$. The function labeled 00 represents the ground-state density while the others represent the change in density for transitions to higher-lying states of the ground-state band. The properties of the ground-state band can be derived from the knowledge of the transition densities. We collect in Table I the calculated values of the rms radius, $B(E2)$, and $B(E3)$ obtained with $\beta = 1.82$ fm.

It is very important also to investigate what happens when the particles are displaced a small amount along the directions of the vectors of normal modes of motion, which are of two types: singly degenerate fully symmetric, A, and doubly

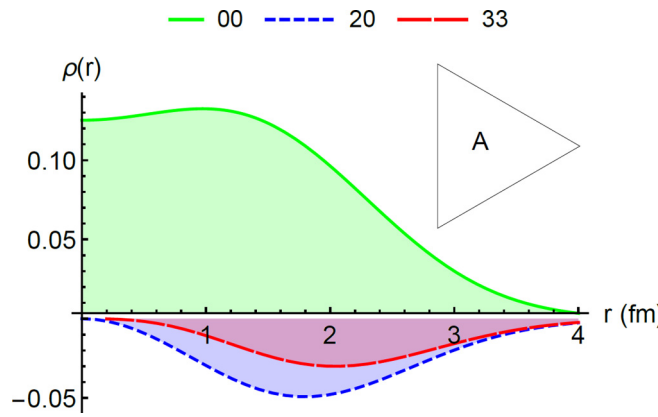

FIG. 3. Radial transition densities, $\rho_{\rm gs}^{\lambda,\mu}$ in Eq. (2) of the ground-state band with A symmetry.

TABLE I. Calculated observables within the ground-state band.

$\langle r^2\rangle^{1/2}_{0^+_1}$	2.45 (fm)
$B(E2; 2^+_1 \to 0^+_1)$	7.86 (e^2 fm^4)
$B(E3; 3^-_1 \to 0^+_1)$	65.07 (e^2 fm^6)
$B(E4; 4^+_1 \to 0^+_1)$	96.99 (e^2 fm^8)

degenerate, E. For example, we can obtain the first symmetric vibrational band of A type (with $n = 1$) by adding a small displacement $\Delta\beta^A$ along the arrows of the inset in Fig. 6. It amounts to redefining the radial variable in $\vec{r}_{1,2,3}$ in Eq. (2) as $\beta + \Delta\beta^A$, namely:

$$A \qquad \vec{r}_k + \Delta\vec{r}^A_k \to \beta + \Delta\beta^A. \tag{9}$$

We should set this displacement by fitting a datum that corresponds to an intrinsic property of the A-vibration band. Unfortunately, neither the radius of the Hoyle state $\langle r^2\rangle^2_{0^+_2}$ nor the transition rate $B(E2; 2^+_2 \to 0^+_2)$ are measured (there are, however, several theoretical calculations). We show the variation of these two quantities with respect to the extent of vibration in Fig. 4. By choosing an intermediate value of $\Delta\beta^A = 1.2$ fm that gives a radius of 3.43 fm (about 1 fm more than the ground state as in Ref. [36]) and a transition rate of about 59.6 e^2 fm^4, which is comparable with the calculations of Ref. [35], we can compute the density of the Hoyle state, shown in Fig. 5. The expansion of this density in spherical harmonics, with an expression analogous to Eq. (2), is given in Fig. 6, where one can see the difference of the $\lambda\mu = 00$ term with respect to the ground state. The central region is depleted and clusterization is more evident.

The transition density connecting the ground-state band with the Hoyle band, with A symmetry, can be obtained as

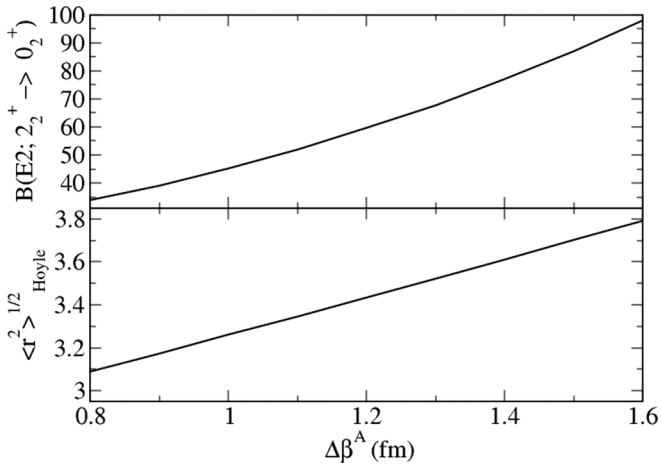

FIG. 4. Calculated values of $B(E2; 2^+_2 \to 0^+_2)$ (upper panel in e^2 fm^4) and $\langle r^2\rangle^2_{0^+_2}$ (lower panel, in fm) as a function of $\Delta\beta^A$.

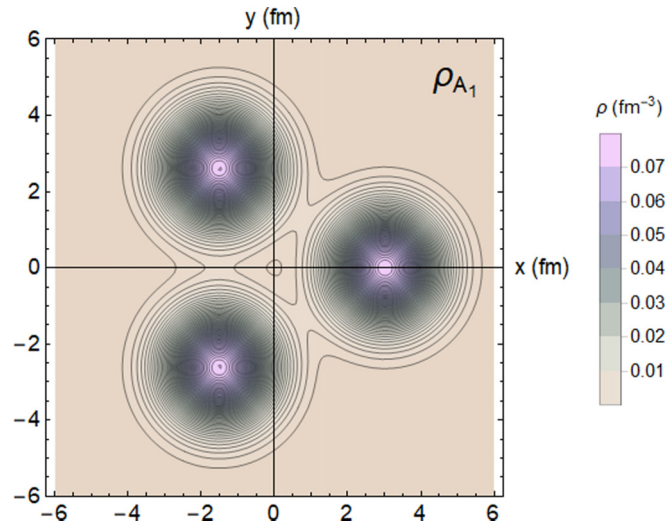

FIG. 5. Density of the Hoyle state, that is, the first A-type vibration in this model, with the α's caught at the moment of maximum elongation.

an expansion in the small displacements at leading order:

$$\delta\rho_{\mathrm{gs}\to A}(\vec{r}) = \chi_1 \frac{d}{d\beta}\rho_{\mathrm{gs}}(\vec{r}, \beta). \tag{10}$$

To calculate the transition rates between the ground-state band and the first excited A-type band, one must set the intrinsic transition matrix element χ_1, akin to the parameter used in Ref. [6], Table I. We set $\chi_1 = 0.247255$ using the value of the monopole matrix element $M(E0)$ in Table II fixed at 5.4 e fm^2, that is, the value measured in Refs. [39,40]. There are other values for this matrix element, namely, in Ref. [41], the isoscalar dipole transition is given as an isoscalar energy-weighted sum-rule strength of $0.08 \pm 0.02(\%)$.

The transition density from the ground-state band to the first excited A band takes the form:

$$\delta\rho_{\mathrm{gs}\to A}(\vec{r}) = \sum_{\lambda\mu} \delta\rho^{\lambda\mu}_{\mathrm{gs}\to A}(r) Y_{\lambda\mu}(\theta, \varphi) \tag{11}$$

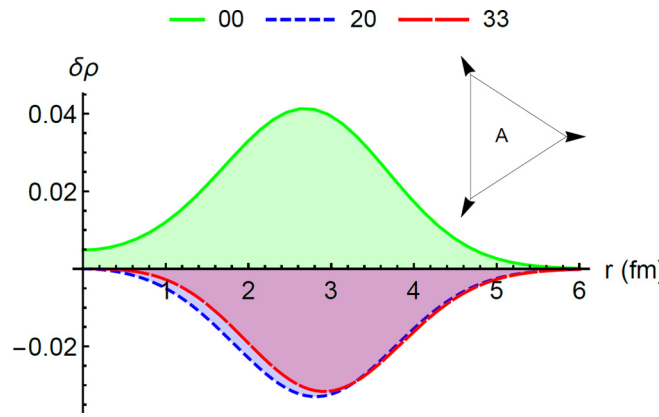

FIG. 6. Radial transition densities, $\delta\rho^{\lambda,\mu}_{gs\to A}(r)$ of Eq. (11), within the excited A band.

TABLE II. Quantities calculated in the present work for the Hoyle band using the values of β and χ_1 given in the text.

$\langle r^2\rangle^{1/2}_{0_2^+}$	3.44 (fm)
$B(E2; 2_2^+ \to 0_1^+)$	0.58 (e^2 fm^4)
$B(E2; 0_2^+ \to 2_1^+)$	2.90 (e^2 fm^4)
$B(E3; 3_2^- \to 0_1^+)$	70.42 (e^2 fm^6)
$M(E0; 0_2^+ \to 0_1^+)$	5.4 (e fm^2)

and this is shown in Fig. 7. The radial components of the expansion in spherical harmonics are shown in Fig. 8 for the allowed values of the projection of the angular momentum $K = 0, 3, 6\cdots$ [5,6]. The cut in Fig. 7 shows the moment at which the particles oscillate away from the center in a synchronous fashion, thus depleting the central region (negative transitions density) and enhancing the external regions (positive transition density). We give in Table II the calculated values for other observables.

Together with the A-type normal mode, there is another doubly degenerate normal mode with E symmetry. The two panels of Fig. 9 show the densities of the doubly degenerate E-type band, whereas the panels of Fig. 10 show the corresponding transition densities. The vector displacements associated with this mode are shown in the insets of Fig. 11. This picture shows the expansion of the densities of the two degenerate components of the 1_1^- state. Now one cannot simplify the notation to the radial variable only as in the preceding case, because these vectors do not point along the radial direction, and therefore in principle one should take:

$$E \quad \vec{r}_k + \Delta\vec{r}_k^E \quad \left|\Delta\vec{r}_k^E\right| \to \eta, \tag{12}$$

but since the direction of the vectors is fixed, we will consider only the magnitude of the displacements, which we call η. In Fig. 9, the amplitude of the vibration has been arbitrarily set to 1.2 fm, i.e., the same value that was used in the A-band to

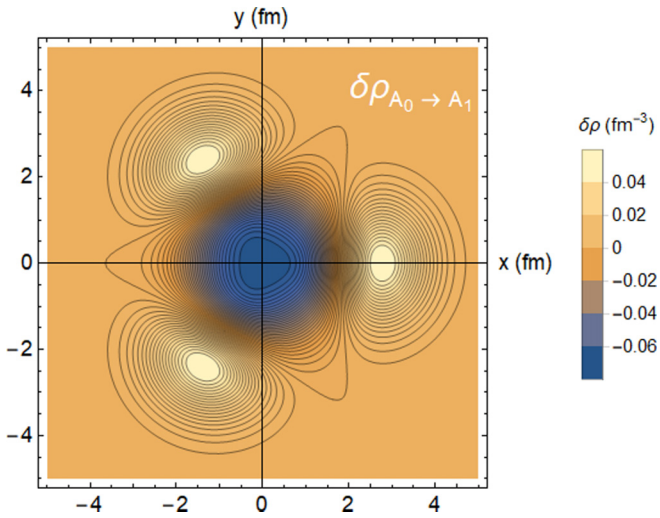

FIG. 7. Transition density for the first A-type vibration.

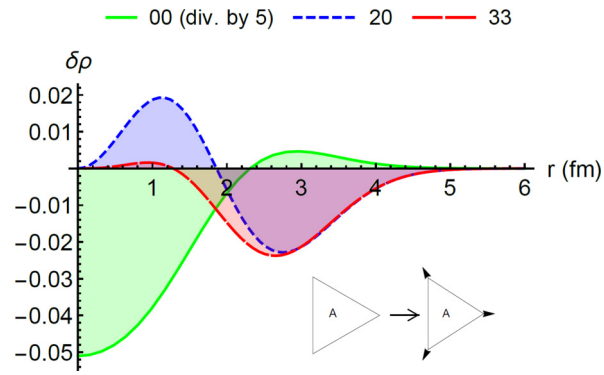

FIG. 8. Transition densities for the first A-type vibration and expansion in the lowest-order spherical harmonics.

set a rms radius about 1 fm larger than in the ground state, for the sake of illustrating the fact that this vibration corresponds to the channel forming ^{8}Be plus an α particle: In fact, in both plots, one of the α's retains its density almost intact and detaches from the rest. With this choice, the rms radius for the

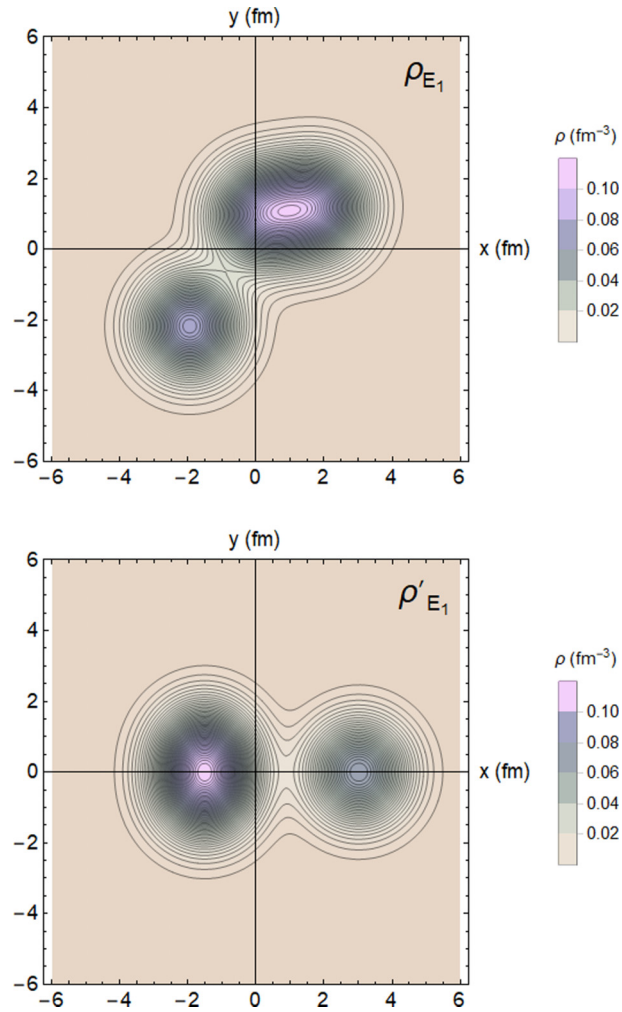

FIG. 9. Densities for the first doubly degenerate E-type vibration. The amplitude of the vibration has been arbitrarily set to 1.2 fm, the same value used for the A band, for the sake of illustration.

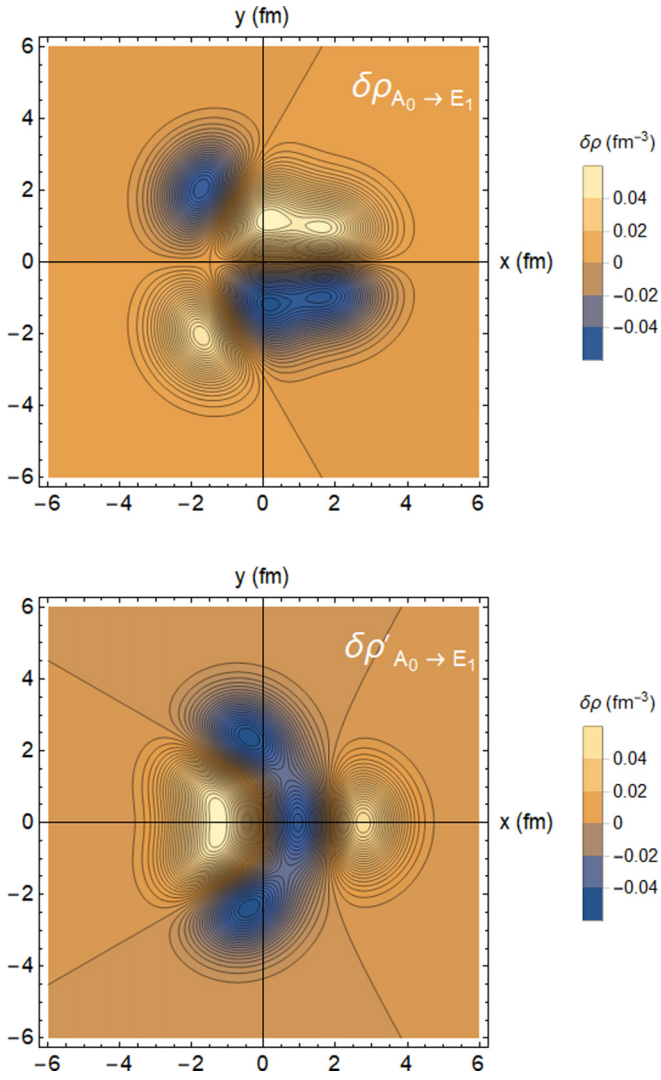

FIG. 10. The doubly degenerate E-type vibrations have two transition densities $\delta\rho$ corresponding to the two normal modes of motions shown in the inset of Fig. 11.

E band is intermediate between the ground-state and Hoyle values.

The intrinsic transition density from the ground to the E band takes a form similar to Eq. (10), namely

$$\delta\rho_{\mathrm{gs}\to E}(\vec{r}) = \chi_2 \frac{d}{d\eta}\rho_{\mathrm{gs}}(\vec{r},\eta), \tag{13}$$

where the value of χ_2 should be set using some experimental observable. This is difficult to accomplish here, as the only information easily accessible is the model-dependent isoscalar dipole matrix element value given in Refs. [35,41] and extracted in α-scattering experiments. In the present case we adopt $\chi_2 = 0.136$ and obtain the value $M(IS1;0_1^+ \to 1_1^-) \simeq 0.31\, e\,\mathrm{fm}^3$. The isoscalar dipole transitions are calculated using the definition of the matrix element as:

$$M(IS1;0_1^+ \to 1^-) = Z \int \delta\rho^1_{\mathrm{gs}\to E}(r)\left(r^3 - \frac{5}{3}\langle r^2\rangle r\right) r^2 dr. \tag{14}$$

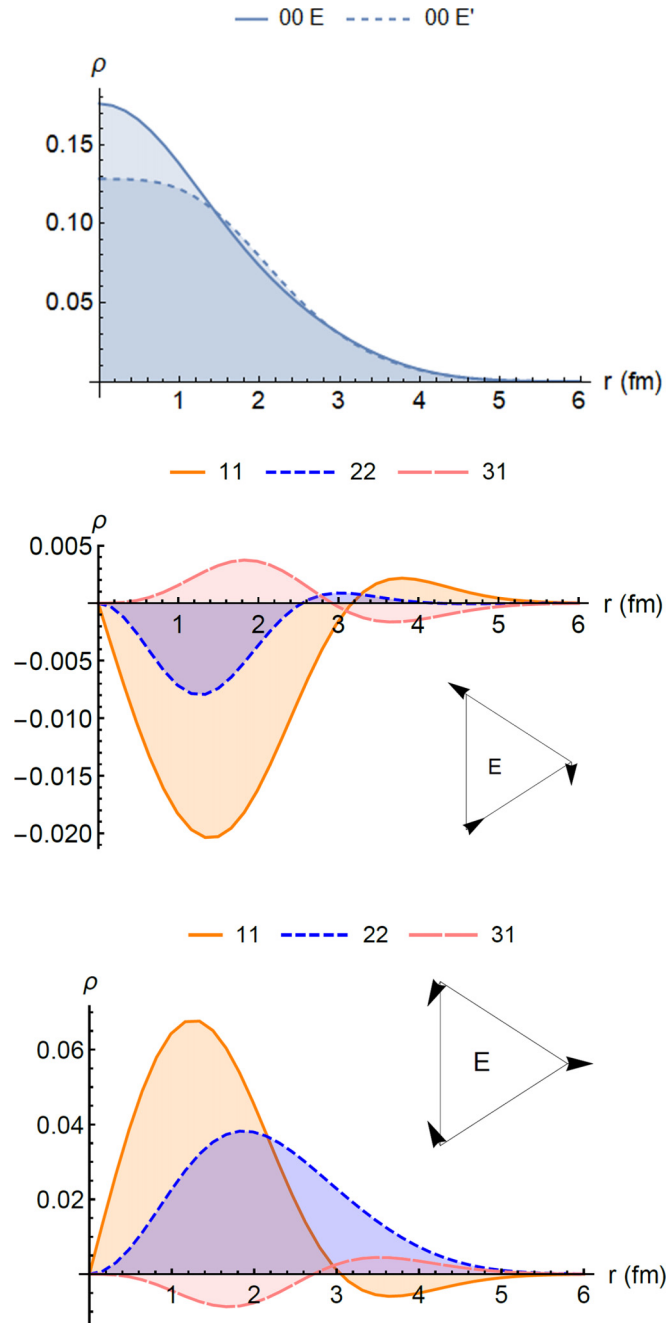

FIG. 11. Densities of the two degenerate modes of the E-type vibration. The two dominating $\lambda\mu = 00$ components are given in the first panel for both degenerate states, while the others are given separately in the second and third panels. Notice the different vertical scales.

The transition densities for the E-type vibrations are expanded in multipoles

$$\delta\rho_{\mathrm{gs}\to E}(\vec{r}) = \sum_{\lambda\mu} \delta\rho^{\lambda\mu}_{\mathrm{gs}\to E}(r) Y_{\lambda\mu}(\theta,\varphi) \tag{15}$$

and the radial part of the transition densities for the first few states, having $K = 1$ or $K = 2$ (and, more in general, all values of K that are not divisible by 3), are shown in Fig. 12.

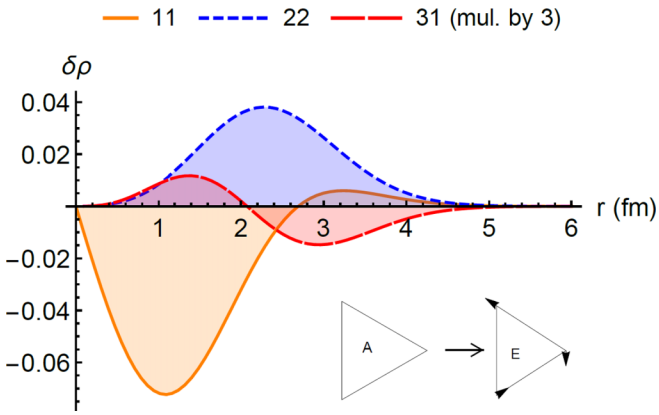

FIG. 12. Radial transition densities $\delta\rho^{\lambda\mu}_{\mathrm{gs}\to E}(r)$ to the E-type band for the first type of motion (inset). The corresponding transition densities for the second type of motion can be obtained by changing sign for 11 and 31.

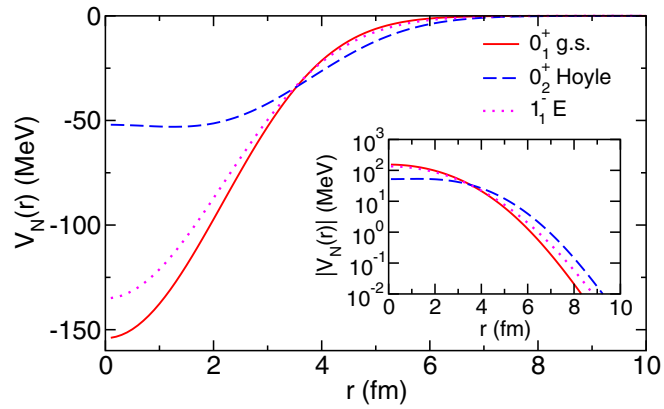

FIG. 13. Double folding nuclear potentials for the system $\alpha + {}^{12}$C for the ground (red dot-dashed line), the "Hoyle" (blue dashed), and the E-type (dotted) band states. The inset shows the same quantity (absolute values) in logarithmic scale to appreciate the different radial extension on the tails.

Notice that the curves are the same for the two degenerate modes. The smaller one, i.e., the $\{\lambda\mu\} = \{31\}$ component, has been magnified three times to make it comparable with the others.

III. FORM FACTORS

The densities and transitions densities described above in the equilateral triangular cluster model contain all the structure information to compute form factors for inelastic excitation processes such as the $\alpha + {}^{12}$C scattering, provided one chooses a suitable *NN* potential. We construct the real part of the nuclear optical model potential using a double-folding prescription as in Refs. [42,43], namely

$$V_N(R) = \iint \rho_\alpha(\vec{r}_1 - \vec{R})\, \rho_T(\vec{r}_2)\, v_N(r_{12})\, d\vec{r}_1 d\vec{r}_2, \qquad (16)$$

where $\rho_{\alpha,T}$ are the densities of projectile and target and the effective interaction v_N is a function of the *NN* distance r_{12}. In this case the α particle is an isoscalar probe ($N = Z$ system); therefore only the isoscalar part of the interaction will contribute to the integral. The widely used density-dependent Reid-type M3Y *NN* interaction is used for v_N [42,44]. Of course, due to the density dependence, the folding potential is different for each combination of projectile and target densities: In our case the α particle is always in the ground state for low energies, while the target can be in any of the selected low-energy states. The potential might differ significantly in the interior but is quite similar on the surface region, as shown in Fig. 13, that is, the relevant one for grazing processes. The potential in the case of the Hoyle state has a slightly longer tail, due to the fact that the densities of Fig. 5 show indeed a larger range with respect to the ground state. In the figure we give also the potential used in the case of the two degenerate 1^- states that are almost identical. The inset shows the same potentials in logarithmic scale to appreciate the differences on the tail.

Using the transition densities calculated above, one can also compute nondiagonal matrix elements and calculate the form factors by double folding:

$$F_{ij}(\vec{R}) = F_{ij}(R) Y_{\lambda\mu}(\hat{R}) = \iint \rho_\alpha(\vec{r}_1 - \vec{R})\, v(r_{12})\, \delta\rho_{i\to j}(\vec{r}_2)\, d\vec{r}_1 d\vec{r}_2, \qquad (17)$$

where v contains the nuclear and coulomb interactions. We show in Fig. 14 a few lowest form factors in linear scale to appreciate the difference in magnitude and range, and we show in Fig. 15 a compilation of form factors in logarithmic scale, where the nuclear and Coulomb contributions are shown together with the total. Clearly, the $0^+_{\mathrm{gs}} \to 0^+_2$ monopole transition has only the nuclear part.

In these figures the excitation processes of interest are those related to the 2^+ states in the ground and "Hoyle" bands. The comparison between the intra- and interband transitions shows that the form factor for the transition from 0^+_2 to 2^+_2 has a larger radial extension than the other two transitions taken into consideration. As a consequence the angular distribution for this transition may cover a reduced angular range com-

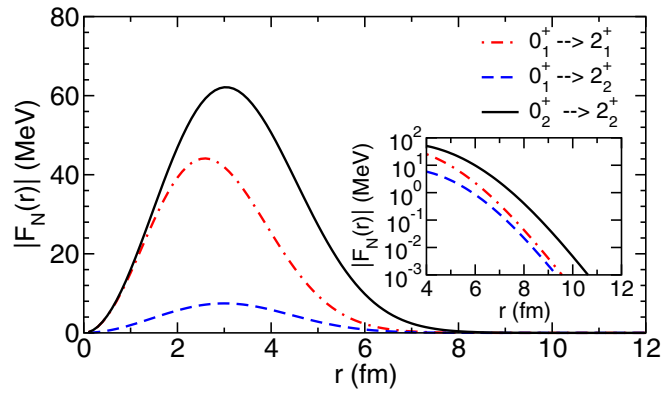

FIG. 14. Absolute value of radial form factor for the system $\alpha + {}^{12}$C for the three excitation processes shown in the legend. The quadrupole states are the one built on top of the ground state (2^+_1) and on top of the 0^+_2 "Hoyle" state (2^+_2).

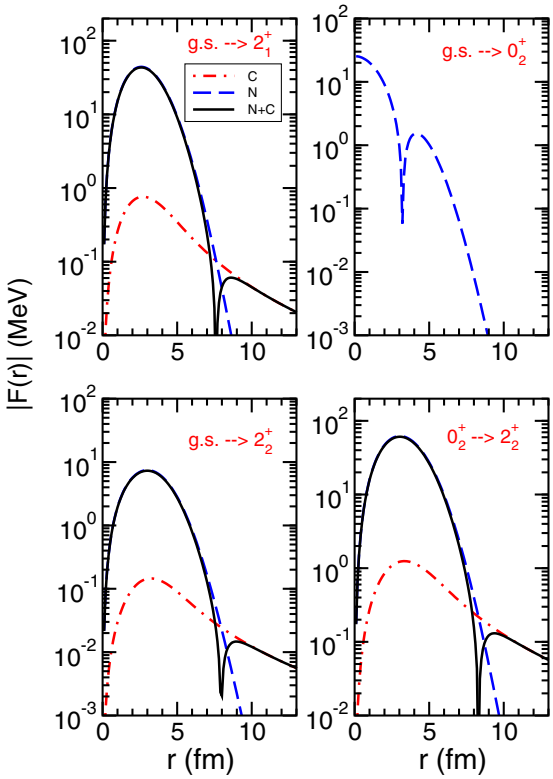

FIG. 15. Form factors in logarithmic scale for a few inelastic excitation processes of interest. We show the nuclear, Coulomb, and total form factors.

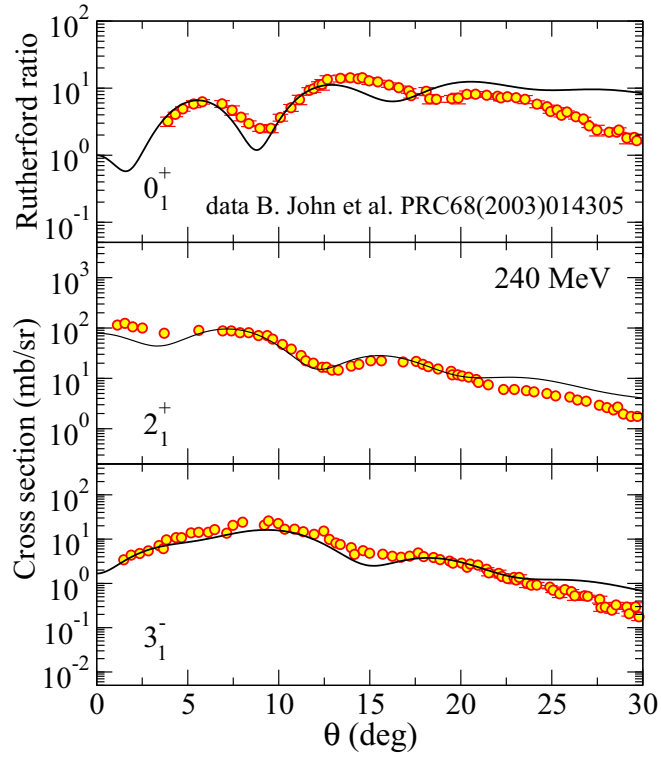

FIG. 16. Differential cross section for the elastic scattering and the transitions $0^+_1 \rightarrow 2^+_1$ and $0^+_1 \rightarrow 3^+_1$ at 240-MeV bombarding energy. Data are from Ref. [41] (retrieved through EXFOR).

pared to the other ones and therefore might give a hint on the radial extension of the 2^+_2 state as pointed out in Ref. [36]. The strong in-band coupling could give rise instead to a significant interference between the direct population of the 2^+_2 state and the two-step process via the 0^+_2 state. This interference, once plugged into a coupled-channels calculation, could give information on the different radial size of the ground and Hoyle bands as a function of scattering angle and bombarding energy.

In order to illustrate that the simple geometrical model is able to capture the main features in reactions where α-cluster degrees of freedom are involved, we have computed DWBA differential cross sections for $\alpha + {}^{12}$C inelastic scattering. In Fig. 16 we show the differential cross section (or ratio to Rutherford in the elastic case) for the ground-state elastic scattering and for the excitation to the first excited 2^+ and 3^- states for the $\alpha + {}^{12}$C reaction. In these calculations we have set the imaginary part of the optical potentials and form factors to 1/2 of the real part. The experimental data [41] are retrieved through the EXFOR database. Among the many possible bombarding energies, we have taken the dataset at 240 MeV as an example of the ability of the α-cluster model to reproduce correctly the shape and magnitude of these cross sections. There is some deviation of the calculated line with respect to the data at angles above the grazing angle, but the overall behavior is well reproduced. These results are encouraging and indicate that, despite the complications that one might invoke in other models, the present simple approach is enough to explain the data, a symptom that α clustering plays a vital role here. In Fig. 17, we give the calculations and data for the $0^+_1 \rightarrow 0^+_2$ transition (ground to Hoyle): In this case we have explored the sensitivity of the DWBA calculations to the depth of the imaginary part of the potential. The three curves (dotted red, solid blue, and dashed black) correspond to the imaginary parts set to 1/4, 1/2, and equal to the depth

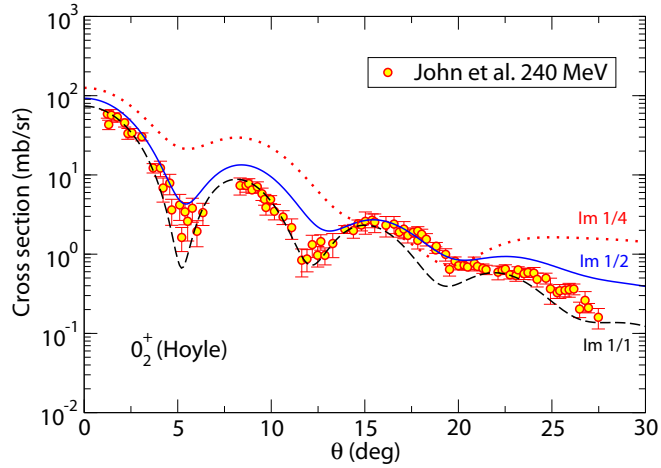

FIG. 17. Differential cross section for the transition $0^+_1 \rightarrow 0^+_2$ at 240-MeV bombarding energy. Data are from Ref. [41] (retrieved through EXFOR) and the three curves have different factors for the depth of the imaginary part as indicated in the figure.

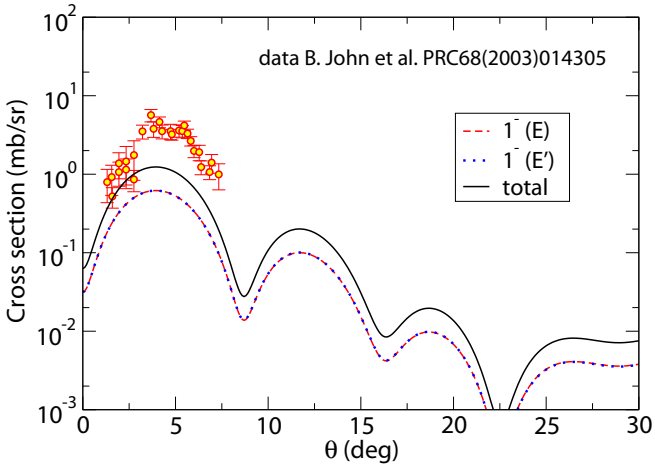

FIG. 18. Differential cross section for the transition $0_1^+ \rightarrow 1_1^-$ at 240-MeV bombarding energy. Data are from Ref. [41] (retrieved through EXFOR). The dashed colored curves show the cross section to the two degenerate components, indicated with E and E' and the black solid curve shows the sum.

of the real part. The shape of the curve is again very good and clearly the best agreement is found for values between 1/2 and 1. This is an indication that not only the description of the ground-state band is good, but also the description of the Hoyle band in terms of breathing vibration finds confirmation in reaction data.

In Fig. 18 we show the differential cross section to the bandhead of the E-type band, that is, the sum of two components. Despite the geometrical differences, the averaged integrals give the same results for the two components. The comparison with data is good at very small angles but fails to reproduce the peak at around 4°–5°. Clearly, this depends on the choice of the χ_2 parameter, which we had previously fixed to the matrix element of the model-dependent isoscalar electric dipole transition. A change by a factor of two (that would take χ_2 to about the same value of χ_1) would reproduce the peak and slightly overestimate the cross section at the smallest angles. We have checked that a change of η within the range 1.0–1.4 does not affect appreciably the final result. Instead, a change in the imaginary part of the potential does change the differential cross section to the 1_1^- state but mostly at larger scattering angles. The change within the extent of the data is not very relevant.

We have confined ourselves to DWBA calculations in the present paper for the sake of illustrating the validity of the approach. Coupled-channels effects show up if one includes higher excited states, as shown in Ref. [37] and in Ref. [45] for the 0_2^+ state, but they are not strictly necessary to the present discussion. For instance, our DWBA calculations do not reproduce the data for the 1_1^- state at angles around 5° in Fig. 18, while they give a reasonable reproduction at smaller angles. The same is observed in Ref. [35], where, in addition, coupled-channels calculations are performed that better fit the existing data. Clearly a simple DWBA approach, based only on the direct transitions from the ground state cannot be satisfactory in the presence of strong second-order couplings. A typical example is the population of the 2_2^+ state in the Hoyle band, where, due to the strong $B(E2; 0_2^+ \rightarrow 2_2^+)$, the direct transition competes with the strong two-step process passing through the 0_2^+ state [36,37].

IV. CONCLUSIONS

We have investigated the performance of the α-cluster model for ^{12}C in reproducing structure and reaction observables. We have set up the densities of the α cluster and the carbon-12 nucleus as an equilateral triangular arrangement according to the recent prescriptions used in the Algebraic Cluster Model. We have constructed transition densities to the states of the ground band and to the states of excited A and E bands. In doing so, we have chosen some parameters to reproduce a minimal set of known matrix elements or electromagnetic transition rates, and we have seen that the model is able to give a quantitative interpretation of almost all the available data. The densities have been used to generate double folding potentials between the α particle and the ^{12}C nucleus. Form factors for several transitions have been computed and used in DWBA calculations to show that this molecular model with a very simple geometry is indeed able to reproduce the shape and magnitude of many scattering data. Notably, the ground-to-Hoyle $0_1^+ \rightarrow 0_2^+$ transition, which involves a static equilateral triangular configuration in the ground state and an oscillating equilateral triangle breathing mode for the Hoyle state, provides a satisfactory explanation for the scattering data if one allows for a slightly deeper-than-usual imaginary part of the optical potential. We have also investigated the cross section to the doubly degenerate E band. Despite the quite significant geometrical differences between the two components of Fig. 9, their form factors and reaction observables look practically the same.

In conclusion, α clusters, if properly described in a fully quantal molecular approach, not only play a role in the Hoyle state, as it was commonly believed until a few years ago, but they are strongly involved in the structure of the ground state and in a large part of the lowest excited states. The role of the fermionic degrees of freedom and the Pauli principle does not seem to be crucial for the description of structure and reactions where the cluster degrees of freedom are involved. In addition to the structure properties, this model can be effectively applied to reaction observables, thus significantly enlarging the amount of data that can be described in the molecular approach that includes rotations and vibrations of a simple triangular cluster configuration.

It is worth noting that the present approach does not take into account the unbound nature of ^{12}C states above the three-α threshold, starting with the Hoyle state. Three-body calculations with α-α scalar interactions, including continuum effects explicitly, could provide more insight into the structure properties of this nucleus. Work along these lines is ongoing and will be presented elsewhere, together with full coupled-channels calculations for the $\alpha + {}^{12}$C inelastic excitation within both approaches, which is definitely essential in the population of, e.g., the 2_2^+ state.

ACKNOWLEDGMENTS

The authors are grateful to Prof. A. Moro (University of Seville, Spain) for his help in setting up FRESCO input files. This work has been supported by SID funds 2019 (Investimento Strategico di Dipartimento, University of Padova, Italy) under Project No. CASA_SID19_1.

APPENDIX

The states in the laboratory frame can be written as

$$|IM, n_A n_E\rangle = \sum_K \underbrace{\sqrt{\frac{2I+1}{16\pi^2(1+\delta_{K,0})}}}_{\mathcal{N}_K} \left[\mathcal{D}^{(I)*}_{MK} + (-1)^K \mathcal{D}^{(I)*}_{M,-K}\right] |n_A n_E\rangle, \tag{A1}$$

where the intrinsic state $|n_A n_E\rangle$ is labeled by the number of phonons of each type, such that the ground state is $|00\rangle$,while the bandheads of the A- and E-type first vibrations are $|10\rangle$ and $|01\rangle$, respectively.

The transition density in the laboratory frame can be related to that into the intrinsic frame with

$$\langle I_f M_f, n_A n_E | \hat{\rho} | I_i M_i, n_A n_E \rangle = \sum_{\lambda\mu} \delta\rho_{\lambda\mu}(r) \sum_{K_i, K_f} \mathcal{N}^*_{K_f} \mathcal{N}_{K_i} \sum_\kappa C Y_{\lambda\kappa}(\theta\varphi), \tag{A2}$$

where the summations are taken on non-negative values of K's and where

$$C = \frac{8\pi^2}{(2I_f+1)} \langle I_f \lambda I_i \mid M_f \mu M_i \rangle [\langle I_f \lambda I_i \mid K_f \kappa K_i \rangle + (-1)^{K_f} \langle I_f \lambda I_i \mid (-K_f) \kappa K_i \rangle + (-1)^{K_i} \langle I_f \lambda I_i \mid K_f \kappa (-K_i) \rangle + (-1)^{K_f + K_i} \langle I_f \lambda I_i \mid (-K_f) \kappa (-K_i) \rangle]. \tag{A3}$$

From this, one can calculate reduced matrix elements and probabilities.

[1] M. Freer, H. Horiuchi, Y. Kanada-En'yo, D. Lee, and Ulf-G. Meißner, Rev. Mod. Phys. **90**, 035004 (2018).
[2] R. R. Betts, Il Nuovo Cimento **110**, 975 (1997).
[3] M. Freer, *Lecture Notes in Physics* (Springer, Berlin, 2014), Vol. 879, Chap. 1.
[4] V. Della Rocca, Ph.D. thesis, Gran Sasso Science Institute, 2017.
[5] V. Della Rocca, R. Bijker, and F. Iachello, Nucl. Phys. A **966**, 158 (2017).
[6] R. Bijker and F. Iachello, Ann. Phys. **298**, 334 (2002).
[7] R. Bijker and F. Iachello, Phys. Rev. Lett. **112**, 152501 (2014).
[8] R. Bijker, J. Phys.: Conf. Ser. **380**, 012003 (2012).
[9] R. Bijker, A. E. L. Dieperink, and A. Leviatan, Phys. Rev. A **52**, 2786 (1995).
[10] D. J. Marín-Lámbarri, R. Bijker, M. Freer, M. Gai, T. Kokalova, D. J. Parker, and C. Wheldon, Phys. Rev. Lett. **113**, 012502 (2014).
[11] G. Stellin. L. Fortunato and A. Vitturi, J. Phys. G **43**, 085104 (2016).
[12] L. Fortunato, G. Stellin, and A. Vitturi, Few-Body Syst. **58**, 19 (2016).
[13] J. A. Wheeler, Phys. Rev. **52**, 1083 (1937).
[14] J. A. Wheeler, Phys. Rev. **52**, 1107 (1937).
[15] W. Wefelmaier, Naturwiss. **25**, 525 (1937).
[16] L. R. Hafstad and E. Teller, Phys. Rev. **54**, 681 (1938).
[17] J. M. Blatt and V. F. Weisskopf, *Theoretical Nuclear Physics* (John Wiley & Sons, New York, 1962).
[18] W. von Oertzen, Nucl. Phys. A **148**, 529 (1970).
[19] E. G. Adelberger, R. E. Marrs, and K. A. Snover, Phys. Rev. C **19**, 1 (1979).
[20] W. von Oertzen, Z. Phys. A **357**, 355 (1997).
[21] M. Milin and W. von Oertzen, Fizika B **12**, 61 (2003).
[22] H. Morinaga, Phys. Rev. **101**, 254 (1956).
[23] A. Tohsaki, H. Horiuchi, P. Schuck, and G. Röpke, Phys. Rev. Lett. **87**, 192501 (2001).
[24] N. B. Nguyen, F. M. Nunes, and I. J. Thompson, Phys. Rev. C **87**, 054615 (2013).
[25] P. Navrátil, J. P. Vary, and B. R. Barrett, Phys. Rev. Lett. **84**, 5728 (2000).
[26] A. C. Dreyfuss *et al.*, Phys. Lett. B **727**, 511 (2013).
[27] Y. Kanada-En'yo, Prog. Theor. Phys. **117**, 655 (2007).
[28] T. Neff and H. Feldmeier, Nucl. Phys. A **738**, 357 (2004).
[29] M. Chernykh, H. Feldmeier, T. Neff, P. von Neumann-Cosel, and A. Richter, Phys. Rev. Lett. **98**, 032501 (2007).
[30] E. Epelbaum, H. Krebs, T. A. Lähde, D. Lee, and Ulf-G. Meißner, Phys. Rev. Lett. **109**, 252501 (2012).
[31] G. Stellin, S. Elhatisari, and U.-G. Meißner, Eur. Phys. J. A **54**, 232 (2018).
[32] Bo Zhou, Y. Funaki, A. Tohsaki, H. Horiuchi, and Z. Ren, Prog. Theor. Exp. Phys. **2014**, 101D01 (2014).
[33] L. Fortunato, Phys. Rev. C **99**, 031302(R) (2019).
[34] M. Kamimura, Nucl. Phys. A **351**, 456 (1981).
[35] D. C. Cuong, D. T. Khoa, and Y. Kanada En'yo, Phys. Rev. C **88**, 064317 (2013).
[36] M. Ito, Phys. Rev. C **97**, 044608 (2018).
[37] Y. Kanada-En'yo and K. Ogata, Phys. Rev. C **99**, 064601 (2019).
[38] A. Vitturi, J. Casal, L. Fortunato, and E. G. Lanza, AIP Conf. Proc. **2150**, 020006 (2019).
[39] P. Strehl and Th. H. Schucan, Phys. Lett. B **27**, 641 (1968).
[40] P. Strehl, Z. Phys. **234**, 416 (1970).
[41] B. John, Y. Tokimoto, Y. W. Lui, H. L. Clark, X. Chen, and D. H. Youngblood, Phys. Rev. C **68**, 014305 (2003).
[42] G. R. Satchler and W. G. Love, Phys. Rep. **55**, 183 (1979).
[43] G. R. Satchler, *Direct Nuclear Reactions* (Oxford University Press, Oxford, 1983).
[44] G. Bertsch, J. Borysowicz, H. McManus, and W. G. Love, Nucl. Phys. A **284**, 399 (1977).
[45] K. Minomo and K. Ogata, Phys. Rev. C **93**, 051601(R) (2016).